


 Cite this: *RSC Adv.*, 2024, **14**, 4692

Exploring borderline S_N1 – S_N2 mechanisms: the role of explicit solvation protocols in the DFT investigation of isopropyl chloride†

 Karine Nascimento de Andrade, ^a Bárbara Pereira Peixoto, ^a
 José Walkimar de Mesquita Carneiro ^b and Rodolfo Goetze Fiorot ^{a*}

Nucleophilic substitution at saturated carbon is a crucial class of organic reactions, playing a pivotal role in various chemical transformations that yield valuable compounds for society. Despite the well-established S_N1 and S_N2 mechanisms, secondary substrates, particularly in solvolysis reactions, often exhibit a borderline pathway. A molecular-level understanding of these processes is fundamental for developing more efficient chemical transformations. Typically, quantum-chemical simulations of the solvent medium combine explicit and implicit solvation methods. The configuration of explicit molecules can be defined through top-down approaches, such as Monte Carlo (MC) calculations for generating initial configurations, and bottom-up methods that involve user-dependent protocols to add solvent molecules around the substrate. Herein, we investigated the borderline mechanism of the hydrolysis of a secondary substrate, isopropyl chloride ($i\text{PrCl}$), at DFT-M06-2X/aug-cc-pVDZ level, employing explicit and explicit + implicit protocols. Top-down and bottom-up approaches were employed to generate substrate–solvent complexes of varying number ($n = 1, 3, 5, 7, 9$, and 12) and configurations of H_2O molecules. Our findings consistently reveal that regardless of the solvation approach, the hydrolysis of $i\text{PrCl}$ follows a loose- S_N2 -like mechanism with nucleophilic solvent assistance. Increasing the water cluster around the substrate in most cases led to reaction barriers of $\Delta H^\ddagger \approx 21 \text{ kcal mol}^{-1}$, with nine water molecules from MC configurations sufficient to describe the reaction. The More O'Ferrall–Jencks plot demonstrates an S_N1 -like character for all transition state structures, showing a clear merged profile. The fragmentation activation strain analyses indicate that energy barriers are predominantly controlled by solvent–substrate interactions, supported by the leaving group stabilization assessed through CHELPG atomic charges.

 Received 3rd January 2024
 Accepted 30th January 2024

 DOI: 10.1039/d4ra00066h
rsc.li/rsc-advances

Introduction

S_N1 and S_N2 are the limiting archetypical mechanisms for nucleophilic substitution reactions. The former, also known as $\text{D}_\text{N} + \text{A}_\text{N}$, involves a stepwise mechanism, while the latter, referred to as $\text{A}_\text{N}\text{D}_\text{N}$, is associated with a concerted process. D_N stands for dissociation of the nucleofuge, while A_N for association of the nucleophile.^{1,2} Substrates with leaving groups (e.g., halides and sulfonates) bonded to saturated secondary carbon atoms can undergo both mechanisms and/or pass by borderline pathways (intermediate processes between the two extremes) depending on the solvent and nucleophile nature. When the

solvent also acts as a nucleophile, the chemical reaction is commonly referred to as solvolysis. Along the continuum between these two mechanisms, the S_N2 may gradually shift toward S_N1 as the transition state develops a carbocation character.^{3–6}

A key factor influencing the gradual transition from S_N1 to S_N2 mechanisms is the solvent activity.³ Some studies describe the solvolysis reactions of secondary substrates following a merged mechanism, exhibiting both S_N1 and S_N2 characteristics.^{5–8} This process often involves active nucleophilic solvent assistance (NSA) in the rate-determining step (sometimes referred as S_N3).^{9,10} While extensive efforts have been devoted to unraveling the intricate effects of solvation in chemical processes, accounting for precise solvent effects into quantum simulations of chemical reactions remains a substantial challenge.^{11–13} An efficient strategy to describe these processes at the atomic level combines explicit and implicit solvation methods.^{14,15} There are two main methodologies for defining the solvent arrangement around a particular solute: top-down and bottom-up.¹⁶ The top-down approach

^aDepartment of Organic Chemistry, Chemistry Institute, Universidade Federal Fluminense (UFF), Outeiro de São João Batista, 24020-141, Niterói, RJ, Brazil.
 E-mail: rodolfofiorot@id.uff.br

^bDepartment of Inorganic Chemistry, Chemistry Institute, Universidade Federal Fluminense (UFF), Outeiro de São João Batista, 24020-141, Niterói, RJ, Brazil

† Electronic supplementary information (ESI) available. See DOI: <https://doi.org/10.1039/d4ra00066h>



begins with simulating the condensed phase using molecular dynamics or Monte Carlo calculations. Subsequently, a selected number of explicit solvent molecules are introduced at a specific distance from the solute, considering relevant interactions (e.g., 3–4 Å) or based to the radial pair distribution function, to be evaluated at the quantum level.^{4,17–20} In the bottom-up approach, explicit solvent molecules are added one by one around the substrate, seeking stable interactions based on the user's chemical intuition or molecular electrostatic potential analysis.^{16,21–25}

Yamabe and co-workers utilized the top-down approach through molecular dynamics simulations to investigate the continuous changes between S_N1 – S_N2 and S_N2 – S_N3 (NSA effect) in reactions with benzylic substrates. Their study demonstrated that the number of water molecules ($n = 9, 11, 17, 23$, and 29) changes the mechanism from S_N1 to S_N2 or S_N3 .⁴ In a similar vein, Fu and co-workers employed this methodology to establish a mechanistic spectrum for glycosylation reactions based on solvent activity, including tightly (S_N2 -character) or loosely (S_N1 -character) associated ion pairs.¹⁸ Fiorot and co-workers employed Monte Carlo calculations to determine the configuration and the number of water molecules around the substrates, with the goal of mapping a non-ionic Prins cyclization mechanism without catalysts in aqueous media. This mechanism is only assessable by explicitly simulating the solvent molecules.¹⁹ Pereira also employed this stochastic generation of solvent configurations to investigate the mechanism for the alkaline hydrolysis of phosphoranes.²⁰ In both cases, the authors determined the number of water molecules based on the radial pair distribution function.^{19,20}

The bottom-up approach is also widely employed in the exploration of reaction mechanism.^{21–25} Shi and co-workers identified that the solvolysis of *tert*-butyl halides (^tBuX) can follow both $D_N + A_N$ or $A_N D_N$ mechanisms, depending on the solvent's attack orientation with respect to the leaving group.²¹ In a similar reaction, simulating $^t\text{BuCl}$ as substrate, Otomo and co-workers found that the solvolysis predominantly follows a dissociative $D_N + A_N$ mechanism, although the concerted one is also feasible.²² Although the authors conducted a meticulous computational investigation regarding the positioning of solvent molecules around the substrates, the identification of both S_N1 and S_N2 reaction mechanisms may be influenced by the orientation and number of water molecules, which are placed according to the user's chemical intuition.²² Similarly, recent studies have applied this methodology to guide the solvent molecules' orientation by the user, exploring various chemical transformations, including α - and β -lapachone isomerization,²³ CO_2 capture by methanol,²⁴ and S_N2 /E2 mechanism competition,²⁵ to cite some.

Despite the exploration of reaction pathways involving explicit solvent molecules in the mentioned works, none of them have proposed an assessment for systems with merged or borderline mechanisms. Furthermore, these approaches are associated with advantages and disadvantages, essentially correlated with computational cost, nature of the potential energy surface, and inadequate descriptions of solute–solvent interactions.^{16,26} The top-down approach, while offering

a comprehensive description of the condensed phase, is often limited by the computational cost. Usually, these methodologies select several solvent molecules to account for the complete effect of the entire solvation shells.¹⁶ To evaluate chemical transformations using quantum methods (e.g., DFT), which allow to properly evaluate the bond-forming/-breaking phenomena, the simulation routine might require large computational resources. On the other hand, the bottom-up approach remarkably influences the rugged nature of the potential energy surface, which can lead to erroneous results or the identification of multiple reaction mechanisms.²⁶ There are some reports of automated methodologies for such an approach; however, they depend on auxiliary packages or user programming mastery.²⁶

Based on these considerations, herein, we explored a reaction significantly influenced by solvent effects: the hydrolysis (solvolysis with water as the solvent) reaction of a secondary substrate. This phenomenon is recognized as a merged or borderline mechanism, displaying characteristics of both S_N1 and S_N2 reactions.^{5–8} Nucleophilic substitution reactions, such as hydrolysis, play pivotal roles in numerous biochemical and synthetic transformations.^{27–29} Our primary goal is to evaluate the nature of borderline mechanisms in the hydrolysis reaction and investigate how the number (n) and the configuration of explicit water molecules influence the overall energy profile and the nature of the transition state structures. We conducted comparative simulations to generate the initial configuration, employing both a top-down approach through Monte Carlo (MC) calculations and a bottom-up protocol known as microsolvation (MS). To the best of our knowledge, this work is the first to delve into comparing these methodologies and evaluating which one yields the more reasonable results. In the microsolvation approach, solvent molecules are strategically introduced to stabilize both the charged nucleophile and nucleofuge. We selected isopropyl chloride as the prototype system because it is the simplest secondary substrate that undergoes hydrolysis reactions by both the S_N1 and/or the S_N2 mechanisms (eqn (1)). The structural simplicity allowed us to focus specifically on the S_N1 – S_N2 mechanistic continuum and evaluate the influence of the explicit solvation methodology.



Methods

All the quantum calculations were performed using the density functional theory (DFT), implemented in the Gaussian 09 (ref. 30) software package, with the default convergence criteria. The hybrid meta-exchange–correlation functional M06-2X³¹ associated with the Dunning double-zeta basis set aug-cc-pVQZ^{32,33} was used for all geometry optimization and frequency calculations. The M06-2X, a highly-nonlocal functional that incorporates the double amount of nonlocal exchange (2X),³¹ was selected as the density functional due to its widespread applications in exploring reaction mechanism, especially when accounting for the solvent effects.^{34–37} The Dunning aug-cc-

pVQZ Gaussian-type basis set has previously been identified as suitable for describing nucleophilic substitution at carbon.³⁸ The choice of a double-zeta basis set over a quadruple-zeta one was driven by the computational cost associated with the simulated systems.³⁹ A brief discussion on the Basis Set Superposition Error (BSSE) and its correction^{40,41} in describing our system is included in the ESI.† Additionally, the M06-2X/aug-cc-pVDZ combination has been previously recommended for calculations involving H-bonded water dimers,⁴² which plays a crucial role in our analyses of hydrolysis reactions. This computational method is implemented in the Gaussian 09. All structures were pre-optimized using the semiempirical tight-binding (TB) method called Geometry, Frequency, Non-covalent, eXtended TB (GFN-xTB)⁴³ aiming to get a better initial guess structure before proceeding to the mechanistic evaluations. The nature of the stationary points was characterized by computing their second-order Hessian matrix. Minimum energy points were identified as those with only positive eigenvalues, while first-order saddle points (TS) with only one negative eigenvalue. In addition, intrinsic reaction coordinate (IRC)⁴⁴ calculations were performed to confirm that each transition structure connects the precedent reactants to their respective products. Thermodynamic parameters were computed at 298 K and 1 atm, after frequency calculation in the default configuration using the standard statistical thermodynamic equations.⁴⁵ The energy profile is reported in terms of the enthalpy (H) change relative to the initial complex (IC) for all the evaluated systems. The reaction enthalpy, ΔH (thermodynamic profile), and the activation enthalpy, ΔH^\ddagger (kinetic profile), are calculated using eqn (2) and (3), where FC refers to the final complex (product), and TS[‡] refers to the transition state structure:

$$\Delta H = H(\text{FC}) - H(\text{IC}) \quad (2)$$

$$\Delta H^\ddagger = H(\text{TS}^\ddagger) - H(\text{IC}) \quad (3)$$

The results in terms of Gibbs free energy (ΔG) and electronic energy change (ΔE) were likewise calculated and are provided in the ESI file (Table S1†).

We assessed two approaches to model the arrangement of water molecules around the substrate for obtaining the initial complex configuration. This involved utilizing the automatic Metropolis Monte Carlo method calculations (MC) performed at DICE software,^{46,47} and employing explicit microsolvation (MS). In the latter, water molecules were inserted into suitable sites to establish interactions with the nucleophile and nucleofuge. The MC calculations were performed only to select initial distribution of solvent molecules around the substrate. For a detailed description of the MC protocol, see the ESI.† In the MS approach, we progressively added the water molecules in each MS calculation two by two: one on the nucleophile site and the other on the leaving group site. Thus, the minimum amount of simulated water molecules was $n = 3$, one as the nucleophile (isopropyl chloride monohydrated) and two as explicit solvent. We also explored $n = 5$ and $n = 7$. The different water molecules configurations were categorized using the microsolvation motif

(l, m) , where l and m denote the number of solvent molecules coordinating around the leaving group and the nucleophile site, respectively.²² In addition, we considered implicit solvation with the self-consistent reaction field (SCRF). The integral equation formalism variant of the polarizable continuum model (IEPCM) was used to simulate the continuous medium of water ($\epsilon = 78.35$).⁴⁸ The combination of explicit solvent molecules and a continuum medium (implicit solvation) is reported as a cluster-continuum model or a mixed discrete-continuum model.^{17,22} In this work, we will refer to this combination as the explicit + implicit model, while the evaluation without implicit solvation will be called only explicit.

To rationalize the nature of the transition structures (tight or loose), we constructed More O'Ferrall-Jencks plots in terms of the C-Cl (leaving group) and C-O_{nuc} (nucleophile) bond orders. The bond orders were calculated based on the Wiberg bond index⁴⁹ using natural bond orbital (NBO)⁵⁰ analysis.

Finally, we employed the activation strain model (ASM)^{51,52} to understand how the number of water molecules affects the reactivity of the secondary halide in S_N reaction. This model decomposes the total electronic energy, $\Delta E(\zeta)$, in terms of interaction, $\Delta E_{\text{int}}(\zeta)$, and strain, $\Delta E_{\text{strain}}(\zeta)$, as represented in the following eqn (4):

$$\Delta E(\zeta) = \Delta E_{\text{int}}(\zeta) + \Delta E_{\text{strain}}(\zeta) \quad (4)$$

Strain (or distortion) is related to the geometrical deformation of the fragments and is typically a destabilizing factor (computed as positive value), whereas the interaction energy is frequently a stabilization factor (computed as negative value, in most cases). The ASM allows for both quantitative and qualitative interpretation of the physical factors that influence the activation barriers. It has been widely used in reaction mechanism studies, particularly in S_N2 processes.^{25,27,53} Here, we conducted energy decomposition along the intrinsic reaction coordinate (IRC) projected onto the C_(electrophilic center)⋯⋯Cl_(leaving group) (C^z⋯⋯Cl) distance using the PyFrag program⁵⁴ on the Gaussian 09 interface.

Results and discussion

The energy barrier for the isopropyl chloride hydrolysis was experimentally determined as $\Delta H^\ddagger = 25.9$ kcal mol⁻¹ at 298 K and 1 atm, determined through quasi-thermodynamic analysis.⁵⁵ This methodology, however, has faced criticism for theoretical inconsistencies.^{55–57} To the best of our knowledge, there are no recent experimental data for the solvolysis reaction. Thus, the available data may be unreliable, emphasizing the importance of investigating solvolysis reactions and their borderline profiles. Herein we examined two different approaches to define initial configurations of the water molecules around the substrate to further investigate the solvolysis reactions: Monte Carlo (MC) and explicit microsolvation (MS) calculations. The former is user-independent, as Metropolis Monte Carlo method generates configurations of the substrate solvated by the water molecules based on stochastic methods and adjusts the arrangement of the molecules during the



simulations. In contrast, the latter is user-dependent as the orientation of the water molecules is defined to establish stabilizing intermolecular interactions. Our results are organized into three sections. First, we discuss the acquisition of the initial configuration through Monte Carlo (MC) and molecular dynamics (MS) explicit solvation approaches. Next, we present the energy profiles (varying the number n of water molecules) for the nucleophilic substitution reaction, addressing the impact of different solvation approaches on the reaction pathways. Finally, we analyze the reactivity of the secondary alkyl halide in the various configurations using the More O'Ferrall-Jencks plot and the activation strain model.

Explicit solvation: exploring initial configurations of substrate–solvent clusters

We started simulating initial complexes (substrate + water cluster) by MC calculations. Further details regarding the Monte Carlo simulation are present in the ESI.† To account for the solvation effects in the cybotactic region (*i.e.*, the interacting water molecules in the first solvation shell), three radial distribution functions (RDFs) were explored to generate the initial structures. The 1st RDF defines the solvation shell from the center of mass of the $^1\text{PrCl}$; the 2nd RDF considers any atoms in the substrate; and the 3rd RDF accounts for the distance of the solvent molecules from the electrophilic carbon atom (Fig. S1, in ESI†). The complete first solvation shell for those RDFs comprises more than 20 solvent molecules. It means that the simulation at the M06-2X/aug-cc-pVDZ level would have a considerably high computational cost (approx. 1100 basis functions). Thus, we decided to take the maximum point of the $G(r)$ and integrate it to obtain the number of water molecules instead of simulating the complete first solvation shell for all the RDFs. It resulted in three substrate–solvent complexes with

$n = 5$ (2nd RDF), 9 (3rd RDF), and 12 (1st RDF) water molecules. Fig. 1a shows the optimized structures (M06-2X/aug-cc-pVDZ) of these MC initial complexes (IC).

Stable three- and five-membered water rings are present in all simulated structures, consistent with previous reports exploring the simulation of a cluster of water molecules.⁵⁸ In neutral solutions, water molecules tend to form cyclic trimers and pentamers as dominant clusters. Interestingly, for the configuration with $n = 5$, the formation of a pentameric stable water cluster prevents the orientation of water molecules on the opposite side of the leaving group, which is a suitable position for the nucleophilic substitution.⁵³ For $n > 5$, there are enough molecules to form stable clusters with an orientation prompt to the nucleophilic attack.

For the user-dependent explicit microsolvation (MS) procedure, the solvent molecules were oriented around the substrate to establish stabilizing interactions, such as hydrogen bonds, with the nucleophilic oxygen atom ($\text{H}_2\text{O}\cdots\text{H}-\text{OH}$) and dipole–dipole interactions with the leaving group from the substrate ($\text{H}-\text{O}-\text{H}\cdots\text{Cl}^{\delta-}$). Progressively, we added two by two water molecules around the substrate: one close to the nucleophile and the other close to the leaving group. Using the microsolvation motif (l, m), where l denotes the number of solvent molecules directly interacting with the leaving group and m denotes the number of molecules interacting with the nucleophilic water, we expected to identify configurations like (1,1) for $n = 3$, (2,2) for $n = 5$ and (3,3) for $n = 7$. For $n = 3$, (1,1) is the only possible configuration that allows the solvation of both nucleophilic water molecule and chloride leaving group. However, for $n = 5$ and $n = 7$, multiple configurations may be obtained as minimum energy points on the PES. A comprehensive discussion regarding these additional configurations is in the ESI file.† The most stable configurations for the IC from the microsolvation approach obtained after full geometry optimization at the M06-2X/aug-cc-pVDZ are shown in Fig. 1b. As the MC and empirical MS approaches result in different amounts of water molecules, a direct correlation between the energy of the individual clusters cannot be established. Thus, our comparison will be limited to the hydrolysis reaction, focusing on variations in the energy barriers.

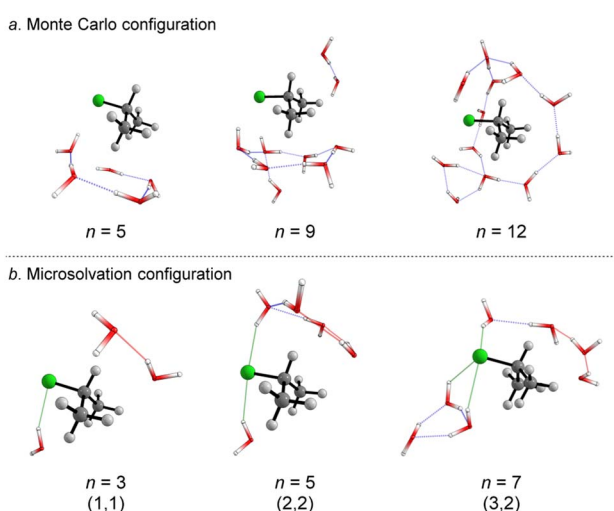


Fig. 1 Optimized structures (DFT-M06-2X/aug-cc-pVDZ) of the initial complexes (IC) from the (a) Monte Carlo ($n = 5, 9, 12$), and (b) microsolvation approach ($n = 3, 5, 7$). For microsolvation configuration, leaving group interaction (l) is highlighted in green and nucleophile interaction in red (m).

Energy profiles for the nucleophilic substitution reactions

We explored the potential energy surfaces for the hydrolysis reaction and identified that in all cases the initial complex (IC) is connected to the final complex (FC) by a first-order saddle point, confirmed by IRC calculations. This suggests that all the processes undergo a $\text{S}_{\text{N}}2$ mechanism, as the $\text{O}\cdots\text{C}(\text{substrate})$ bond formation occurs concertedly (but not synchronously, as we will explore in the next section) to the $\text{C}\cdots\text{Cl}$ bond breaking. All enthalpy changes (ΔH and ΔH^\ddagger) in the energy diagram were calculated relative to their respective initial complex obtained by MC or MS approach. In addition, we also explored the solvolysis in the absence of explicit solvent ($n = 1$), *i.e.* the monohydrated substrate.

Monte Carlo configurations

Fig. 2 illustrates enthalpy changes (in kcal mol⁻¹) for the hydrolysis reaction, considering the initial configurations of



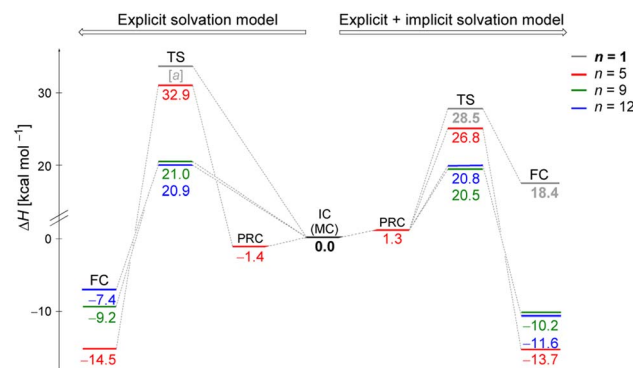


Fig. 2 Enthalpy change (in kcal mol^{-1}) of the hydrolysis reaction of iPrCl using the initial configurations of substrate–solvent clusters generated by Monte Carlo simulations. Left side displays the results obtained using exclusively explicit solvation model, and right side displays combined explicit + implicit solvation model results. Computed relative energies relative to their respective initial complexes, IC, at DFT-M06-2X/aug-cc-pVDZ level. TS refers to the transition state, PRC to pre-reactive complex, and FC to the final complex (products). [a] TS could not be optimized probably due to the necessity of stabilizing the charged leaving group, Cl^- , by explicit solvent or a continuum medium.

substrate–solvent clusters generated by Monte Carlo (MC) calculations with $n = 5, 9, 12$. The left side displays results obtained using exclusively the explicit solvation model, that is, without the implicit simulation of the solvent as a continuum medium. On the right side, both explicit and implicit solvation models were employed. The energy of the transition state, identified as TS and the energy of the products, represented by a final complex (FC) were calculated relative to the initial complex (IC, center of the image), representing the activation enthalpy (ΔH^\ddagger) and the reaction energy (ΔH) for each n , respectively.

The data indicate that for $n = 9$ and 12 , the activation energy (ΔH^\ddagger) and reaction enthalpy (ΔH) have nearly identical values for both the explicit and explicit + implicit solvation models. Therefore, according to our findings, when simulating a substantial number of water molecules, there are no noteworthy deviations in the energy profile, resulting in convergent barriers of approximately 21 kcal mol^{-1} . Among all the assessed configurations, $n = 5$ exhibited the highest activation barrier. In this case, the IC configuration (Fig. 1) does not have a water molecule suitably positioned to act as a nucleophile. Thus, we computed an extra stationary point (pre-reactive complex, PRC), with a water molecule in the backside of the leaving group (see Fig. S3, in ESI†). This structure was further confirmed by IRC calculation of the respective TS. Although this rearrangement of solvent molecules breaks the stable cyclic water pentamer,⁵⁸ the number of hydrogen bonds is preserved. Consequently, the change in the relative enthalpy values is almost negligible ($\Delta H = -1.4 \text{ kcal mol}^{-1}$ for the explicit solvation and $+1.3 \text{ kcal mol}^{-1}$ for the explicit + implicit solvation model compared to the $\text{IC}_{n=5}$).

The structural analysis of the TS for each system allows us to infer that there is a progressive decrease in the computed barrier height value as the leaving group establishes more

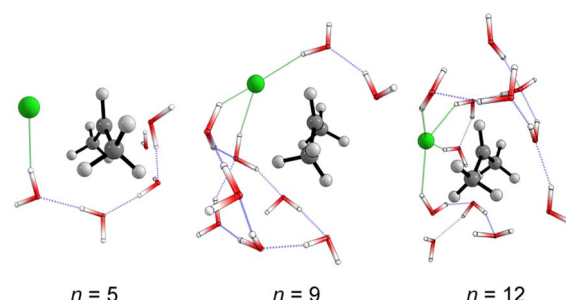


Fig. 3 Optimized (M06-2X/aug-cc-pVDZ) transition states structures obtained from Monte Carlo simulations. Solvent-leaving group interactions are highlighted in green.

interactions with the water molecules (Fig. 3). The TS for $n = 5$ has only one ion-dipole interaction, $\text{Cl}^\delta- \cdots \text{H-OH}$, being the most energetic for both explicit and explicit + implicit solvation models. For $n = 9$ and 12 , three and four water molecules stabilize the leaving group, respectively. These interactions allow for charge density dispersion for the chloride anion, reducing the activation energy. The highest barrier is relative to $n = 1$, since no water molecules are able to interact with the anionic leaving group. It was not possible to locate the TS without simulating the continuum model, probably due to the necessity of the charge on the chloride anion to be stabilized by explicit solvent or a continuum medium (Fig. 2, TS [a]).

The calculated atomic charges of the leaving group on the TS structures corroborate our hypothesis regarding chloride charge stabilization (Fig. 4). The increase in the number of water molecules is followed by the reduction of the charge density of the nucleofuge ($\text{Cl}^\delta-$) in the TSs. In the overall comparison between the explicit and explicit + implicit models, an important decrease in atomic charges is observed in the explicit model, potentially attributed to the strong stabilization provided by explicit solvent molecules. This indicates that in the absence of a continuum medium, the intrinsic interactions between solvent molecules and the substrate become more influential. In the case of the monohydrated substrate ($n = 1$), the explicit + implicit model exhibited the highest charge localization on the chloride atom (no transition state was found in the explicit model). This highlights the importance of explicit water molecules in stabilizing the nucleofuge and facilitating long-range solvation.

Microsolvation configurations

Fig. 5 displays the computed enthalpy change for the systems obtained using the microsolvation approach. Like the MC configurations, a convergence is observed towards the 21 kcal mol^{-1} range for $n = 5$ (both explicit and explicit + implicit models) and $n = 7$ (explicit + implicit model). Notably, the simulation with the minimum number of water molecules, $n = 3$ (indicated in red), exhibits the highest deviation from these values, with an activation enthalpy of $\Delta H^\ddagger = 29.5 \text{ kcal mol}^{-1}$ for the only explicit solvation model and $24.9 \text{ kcal mol}^{-1}$ for the explicit + implicit model.



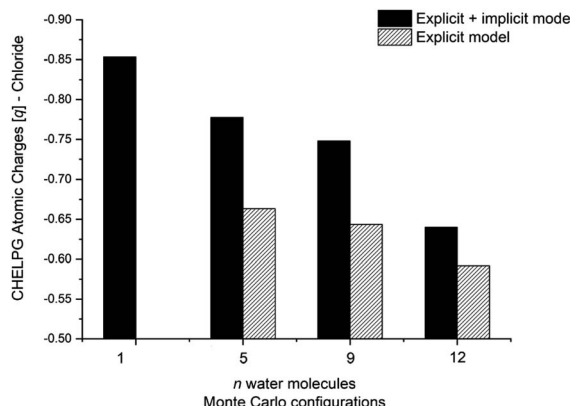


Fig. 4 CHELPG atomic charge calculation (M06-2X/aug-cc-pVDZ) of the nucleofuge ($\text{Cl}^{\delta-}$) on transition state structures of MC configuration. Filled bar represents explicit + implicit model and striped the explicit model. Transition state for $n = 1$ (explicit model) not found.

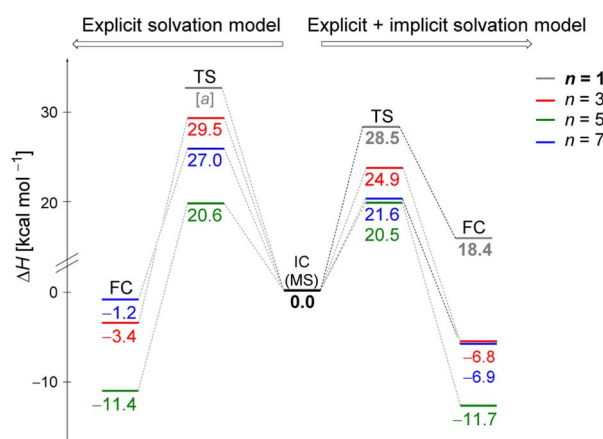


Fig. 5 Enthalpy change (in kcal mol^{-1}) of the hydrolysis reaction of PrCl using the initial configurations of substrate–solvent clusters obtained from explicit microsolvation simulations. Left side displays the results obtained using exclusively explicit solvation model, and right side displays combined explicit + implicit solvation model results. Computed relative energies relative to their respective initial complexes, IC, at DFT-M06-2X/aug-cc-pVDZ level. TS refers to the transition state, PRC to pre-reactive complex, and FC to the final complex (products). [a] TS could not be optimized probably due to the necessity of stabilizing the charged leaving group, Cl^- , by explicit solvent or a continuum medium.

For $n = 5$, the energy barriers exhibit identical values when employing both the explicit and explicit + implicit models. This suggests that solvent orientation alone is sufficient to describe both the direct interaction and the stabilization attributed to the continuum medium. Along the reaction coordinate, the orientation of water molecules can facilitate leaving group stabilization (by two solvent molecules) as well as provide the appropriate direction to promote the solvolysis reaction.

One could expect with an increase in the number of water molecules, there would be a gradual stabilization of the charged transition state through interactions between water and the leaving group. However, it is interesting to note that for $n = 7$

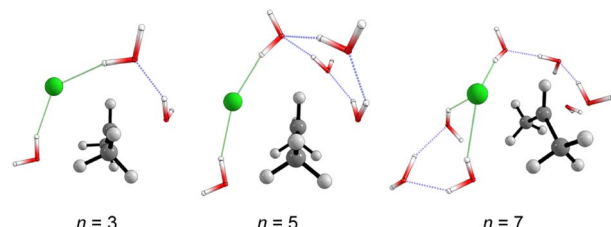


Fig. 6 Optimized transition states structures (M06-2X/aug-cc-pVDZ) obtained from the explicit microsolvation approach. Solvent-leaving group interactions are highlighted in green.

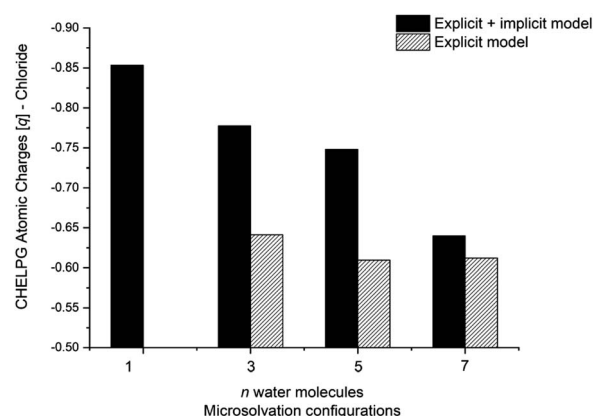


Fig. 7 CHELPG atomic charge calculation (M06-2X/aug-cc-pVDZ) of the nucleofuge ($\text{Cl}^{\delta-}$) on transition state structure of MS configuration. Filled bar represents explicit + implicit model and striped the explicit model. Transition state for $n = 1$ (explicit model) and 23 (explicit + implicit model) not found.

(Fig. 5 in blue, left) in the explicit solvation model, a high energy barrier is observed. Surprisingly, the CHELPG calculations depicted in Fig. 7 reveal no change in the chloride atomic charge from $n = 5$ to 7 in the explicit model.

This suggests that the barrier height is likely not significantly influenced by chloride charge stabilization, in contrast to the observations from the MC approach. To further investigate the differing effects of each solvation approach modeled, we explore these reaction profiles using the activation strain model in the subsequent section.

Reactivity analysis

The number and the arrangement of the simulated water molecules play an important role in the position of the solvolysis reaction on the $\text{S}_{\text{N}}1$ – $\text{S}_{\text{N}}2$ mechanistic continuum. Some solvent orientations for a front or backside pathway can lead to $\text{S}_{\text{N}}1$ ($\text{D}_\text{N} + \text{A}_\text{N}$) or $\text{S}_{\text{N}}2$ ($\text{A}_\text{N}\text{D}_\text{N}$) mechanism due to the charge stabilization of the intermediate.²² It is known, however, that the backside- $\text{S}_{\text{N}}2$ is preferred over frontside- $\text{S}_{\text{N}}2$ for reactions at electrophilic carbon.^{27,38} From our simulations, all the TSs point to a backside $\text{A}_\text{N}\text{D}_\text{N}$ ($\text{S}_{\text{N}}2$ -like) process. To find the TS starting guesses, we performed a relaxed scan calculation elongating the $\text{C}_\alpha \cdots \text{Cl}$ bond. Following this strategy, no water molecule approached the electrophilic carbon to promote a frontside nucleophilic attack. From



the IRC calculations (either for MC or MS), shown in Fig. S5 and S6 in ESI,† the nucleophilic solvent assistance (NSA) is clear. Thus, according to our simulations, the hydrolysis reactions follow an $A_N D_N$ -NSA mechanism, with more than one solvent molecule interacting with the nucleophilic water molecule in the TS structure. From the TS structures (Fig. 3 and 6), we can identify a strict S_{N3} profile for $n = 3$ (MS), and for $n = 5$ and 9 (MC), as defined by Bentley.⁹ For $n = 12$ (Fig. 3), the nucleophile is assisted by three water molecules, and for $n = 5$ and 7 (Fig. 6), by two solvent molecules. Using the $S_{N}X$ nomenclature, these reactions would be termed S_{N5} and S_{N4} , respectively, which could promote kinetic misleading interpretations, since the solvent concentration is constant along the chemical process. Besides that, this reaction profile presents characteristics of S_{N1} , S_{N2} , and $S_{N}X$ ($X = 3, 4, 5$) mechanisms. So, for this system, we could not fit the reaction in terms of the S_{N1} – S_{N2} and S_{N2} – S_{N3} spectrum. The $A_N D_N$ -NSA term fits better in this case.

The More O'Ferrall–Jencks^{59,60} diagrams were plotted (Fig. 8) for each system to position the mechanism closer to the S_{N2} ($A_N D_N$) mechanistic limit, that is, with a tight TS, in which the nucleophile and nucleofuge intimately associated with the electrophilic carbon atom, C^α ; or closer to the S_{N1} ($D_N + A_N$) mechanistic limit, that is, with a loose TS, with nucleophile and nucleofuge more distant to C^α .

All transition states show a remarkable dissociative character, meaning that the $C^\alpha\cdots Cl$ bond dissociation occurs earlier than the $C\cdots O_{Nu}$ bond association, even though the IRC confirm their nature as a concerted mechanism. Transition states of this type are known as loose, in which the electrophilic center has a high electron deficiency and resembles a carbocation. Processes with this type of saddle points are characterized by flat potential energy surfaces,²² which can be visualized on the IRC diagrams (Fig. S7–S9†). The highly dissociative nature observed in the loose transition state suggests that the reaction mechanism exhibits intermediate characteristics of the archetypal borderline models S_{N1} and S_{N2} . Consequently, these reactions can be classified as mixed or intermediate, falling between the two extremes.

Finally, we employed the ASM to gain quantitative insight into how the different solvation models affect the barrier height (ΔE^\ddagger) in terms of the distortion of the substrate (fragment 1) and the water clusters (fragment 2), $\Delta E_{\text{strain}}(\zeta)$, and the magnitude of their interaction $\Delta E_{\text{int}}(\zeta)$. To understand the intrinsic effect of explicit solvation, we evaluated only the explicit solvation model. Fig. 9 presents the activation strain diagrams (ASDs) for the MC and MS configurations.

For each system, we analyzed the strain and interaction contribution along all the reaction coordinates. A single-point analysis at the TS can provide misleading conclusions,⁶¹ once the TSs occurs at different reaction coordinates (*i.e.*, different $C\cdots Cl$ interatomic distances) for each system. We chose the $C\cdots Cl$ interatomic distance at $d_{C\cdots Cl} = 2.61 \text{ \AA}$ as the consistent geometry (*c.g.* in Fig. 9) to compare with the other systems. Regardless of the assessed solvation approach, one can see that as the number of water molecules increase, the interaction (ΔE_{int}) becomes more stabilizing. Overall, as the number of water molecules increases for both solvation approaches, the computed energy barrier

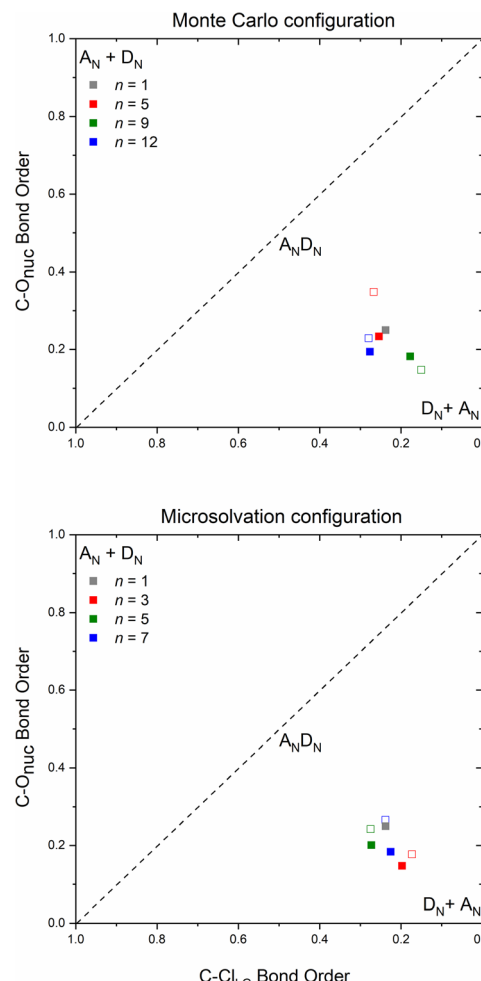


Fig. 8 More O'Ferrall–Jencks diagram in terms of $C\text{--}Cl_{LG}$ and $C\text{--}O_{Nu}$ bond order of the transition state structures obtained by Monte Carlo and microsolvation. Filled squares refer to the optimized TS from the explicit + implicit solvation model and hollow squares to the only explicit model.

values decrease. This suggests that the solvent–substrate interaction determines the barrier height, influenced by both the leaving group interaction and solvation energy of the substrate.

Regarding the MS configurations (Fig. 9b), the interaction curves for $n = 5$ and 7 almost overlap. This agrees with the CHELPG calculations (Fig. 7), as the chloride charge on TS using explicit solvation is the same for $n = 5$ and 7. Thus, the differences in the energy barriers are associated with the strain energy change. For this case, it comes from the more destabilizing distortion of the water cluster for $n = 7$ compared to $n = 3$ and 5 (see Fig. S4, ESI†). The imposed geometry for seven water molecules is associated with a notable distortion along the reaction pathway, which is not observed for $n = 5$, as there is a small water reorganization along the reaction path. Noteworthy, the highest energy barrier for $n = 3$ is caused by a less stabilizing interaction between the fragments along the entire reaction coordinate. It suggests that the three water molecules are insufficient to promote effective interaction between solvent and substrate.



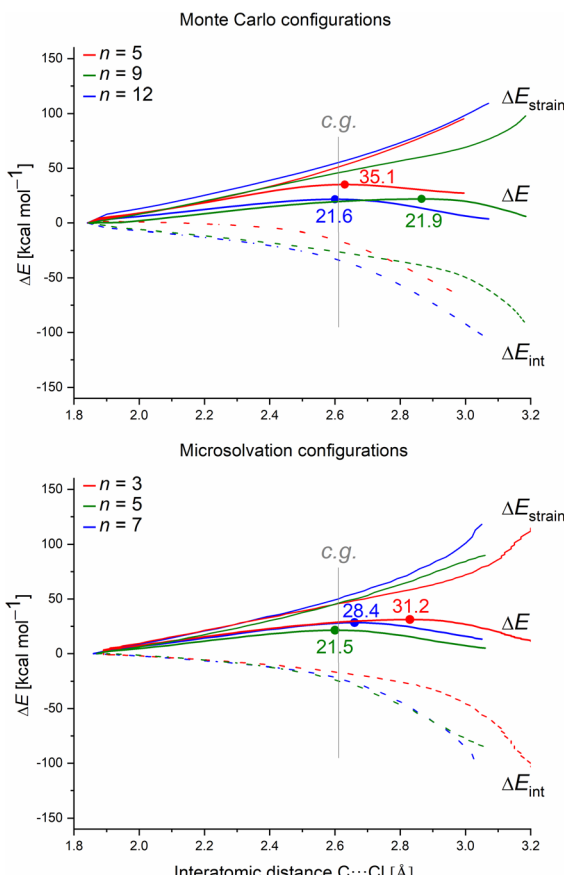


Fig. 9 Activation strain diagrams (ASDs) of the solvolysis reaction along all the intrinsic reaction coordinate (IRC) projected onto the C···Cl interatomic distance (in Å) for the Monte Carlo and microsolvation configurations in the explicit solvation model. Solid bold curves represent the electronic energy change (ΔE), solid light curves represent the strain contribution (ΔE_{strain}), and dashed curves represent the interaction energy change (ΔE_{int}). The dots locate the transition states. Consistent geometry at $d_{\text{C}\cdots\text{Cl}} = 2.61 \text{ \AA}$ (vertical gray line).

Comparing the MC and MS solvation approaches, the former allows the formation of ICs by which the solvolysis reaction occurs without significant changes in the water clusters (pointing by a higher influence of interaction, *e.g.* leaving group charge stabilization rather than strain). On the other hand, for the empirical MS configurations, there is a higher strain influence and no direct correlation with the leaving group charge stabilization. Since we impose the orientation of the solvent molecules around the substrate, the MS approach is highly user-biased. Despite the energy barriers and the nature of the TSs presenting the same profile for the two approaches (about 21 kcal mol⁻¹ and loose TSs), we consider that the user-biased character of MS can provide misleading interpretations and needs to be done cautiously.

Conclusions

We quantum-chemically explored the hydrolysis of the secondary substrate, isopropyl chloride. This reaction is described as a nucleophilic substitution that deviates from the

limiting pathways $\text{S}_{\text{N}}1$ ($\text{D}_\text{N} + \text{A}_\text{N}$) or $\text{S}_{\text{N}}2$ ($\text{A}_\text{N}\text{D}_\text{N}$), lying within the borderline mechanism. To account for the solvent effects, we employed two explicit solvation approaches to generate initial configurations for the substrate–solvent clusters: Monte Carlo (MC) calculations and empirical microsolvation (MS). These protocols yielded different number (n) and configuration of water molecules around the substrate.

Notably, in contrast to the MC approach, the results from the MS approach demonstrated a high level of user bias, as solvent molecules are added based on the user's chemical intuition to establish stabilizing interaction with both the leaving group and the nucleophile. Our findings consistently reveal that, despite the solvation approach, the reaction follows $\text{S}_{\text{N}}2$ -like ($\text{A}_\text{N}\text{D}_\text{N}$) mechanisms in all cases, with the computed energy barrier values converging to 21 kcal mol⁻¹, as the solvent cluster increases. Notwithstanding a concerted $\text{S}_{\text{N}}2$ -like mechanism with a significant nucleophilic solvent assistance, the More O'Ferrall–Jencks plot revealed loose transition state structures, with carbocation character, corroborating the borderline nature of these mechanisms.

Finally, the results from the fragmentation activation strain analyses strongly suggest that the interaction between substrate and solvent molecules plays an important role in controlling the energy barriers. As the number of water molecules increases, a more stabilizing interaction with the substrate along the reaction coordinate is observed, supported by the leaving group stabilization assessed through CHELPG atomic charge calculations. The strain (distortion) curve becomes more significant for configurations obtained from empirical MS, suggesting that the imposition of the water molecules in the IC causes a more pronounced reorganization of the fragments along the reaction, once again evidencing the high bias in this user-dependent method.

We intend to apply this computational protocol to assess the solvent influence on the reactivity of other secondary substrates, such as the congener isopropyl halides. The explicit solvation obtained from the Monte Carlo calculations and the n amount of water extracted from the highest $G(r)$ value of the RDF calculated from the distance between the reactive sites provided us with suitable descriptions of the initial configurations. Besides that, the activation strain analysis and More O'Ferrall–Jencks plot proved to be useful to understand physical features commanding the reactive patterns. Thus, we show a consistent computational methodology to evaluate reaction mechanisms in solvent media that can be applied to comprehend solvent effects on fundamental reactions in organic chemistry.

Author contributions

KNA contributed to conceptualization, methodology, performed investigation, formal analysis, and participated in writing and reviewing the original draft. BPP contributed to investigation and formal analysis. JWMC was responsible for funding acquisition and conceptualization. RGF contributed to conceptualization, project administration, supervision, methodology, and participated in writing and reviewing the original draft.



Conflicts of interest

There are no conflicts to declare.

Acknowledgements

The theoretical calculations were performed using the Lobo Carneiro supercomputer from Núcleo Avançado de Computação de Alto Desempenho (NACAD), under Project ID a20006 and the datacenter OSCAR of Federal Fluminense University. The authors are grateful to CAPES (Coordenação de Aperfeiçoamento de Pessoal de Nível Superior), CNPq (Conselho Nacional de Desenvolvimento Científico e Tecnológico, 309080/2015-0 and 434955/2018-3), and FAPERJ (Fundação Carlos Chagas Filho de Amparo à Pesquisa do Estado do Rio de Janeiro, E-26/203.001/2017, E-26/010.101118/2018, E-26/010.001424/2019, E-26/211.517/2021, and E-26/200.227/2023) for funding this research project.

References

- 1 F. A. Carey and R. J. Sundberg, *Advanced Organic Chemistry – Part A: Structure and Mechanisms*, Springer, New York, 5th edn, 2007.
- 2 E. Uggerud, *Adv. Phys. Org. Chem.*, 2017, **51**, 1–57.
- 3 T. B. Phan, C. Nolte, S. Kobayashi, A. R. Ofial and H. Mayr, *J. Am. Chem. Soc.*, 2009, **131**, 11392–11401.
- 4 S. Yamabe, G. Zeng, W. Guan and S. Sakaki, *J. Comput. Chem.*, 2014, **35**, 1140–1148.
- 5 R. M. Pagni, *Found. Chem.*, 2011, **13**, 131–143.
- 6 T. W. Bentley, C. T. Bowen, D. H. Morten and P. v. R. Schleyer, *J. Am. Chem. Soc.*, 1981, **103**, 5466–5475.
- 7 F. L. Schadt, T. W. Bentley and P. v. R. Schleyer, *J. Am. Chem. Soc.*, 1976, **98**, 7667–7675.
- 8 T. W. Bentley and P. v. R. Schleyer, *J. Am. Chem. Soc.*, 1976, **98**, 7658–7666.
- 9 T. W. Bentley, R. O. Jones, D. H. Kang and I. S. Koo, *J. Phys. Org. Chem.*, 2009, **22**, 799–806.
- 10 T. W. Bentley, H. Choi, I. S. Koo and D. N. Kevill, *J. Phys. Org. Chem.*, 2017, **30**, e3585.
- 11 L. Xu and M. L. Coote, in *Annual Reports in Computational Chemistry*, ed. D. A. Dixon, Elsevier, Amsterdam, 2022, vol. 18, ch. 2, pp. 53–121.
- 12 Y. P. Chin, N. W. See, I. D. Jenkins and E. H. Krenske, *Org. Biomol. Chem.*, 2022, **20**, 2028–2042.
- 13 K. N. de Andrade, J. R. D. Fajardo, C. A. Leal, J. W. M. Carneiro and R. G. Fiorot, *J. Braz. Chem. Soc.*, 2023, **34**(6), 755–895.
- 14 J. Zhang, H. Zhang, T. Wu, Q. Wang and D. van der Spoel, *J. Chem. Theory Comput.*, 2017, **13**, 1034–1043.
- 15 J. R. Pliego and J. M. Riveros, *Wiley Interdiscip. Rev.: Comput. Mol. Sci.*, 2020, **10**, e1140.
- 16 M. Steiner, T. Holzknecht, M. Schauperl and M. Podewitz, *Molecules*, 2021, **26**, 1793.
- 17 J. R. Pliego and J. M. Riveros, *J. Phys. Chem. A*, 2001, **105**, 7241–7247.
- 18 Y. Fu, L. Bernasconi and P. Liu, *J. Am. Chem. Soc.*, 2021, **143**(3), 1577–1589.
- 19 R. G. Fiorot, G. Rambabu, V. Vijayakumar, Y. B. Kiran and J. W. M. Carneiro, *J. Braz. Chem. Soc.*, 2019, **30**(8), 1717–1727.
- 20 E. S. Pereira, J. C. S. Da Silva, T. A. S. Brandão and W. R. Rocha, *Phys. Chem. Chem. Phys.*, 2016, **18**, 18255–18267.
- 21 H. A. Shi, *React. Kinet., Mech. Catal.*, 2020, **129**, 583–612.
- 22 T. Otomo, H. Suzuki, R. Iida and T. Takayanagi, *Comput. Theor. Chem.*, 2021, **1201**, 113278.
- 23 M. Delarmelina, C. D. Nicoletti, M. C. Moraes, D. O. Futuro, M. Buhl, F. C. da Silva, V. F. Ferreira and J. W. M. Carneiro, *ChemPlusChem*, 2018, **84**, 52–61.
- 24 K. N. de Andrade, L. M. da Costa and J. W. M. Carneiro, *J. Phys. Chem. A*, 2021, **125**, 2413–2424.
- 25 T. Hansen, J. C. Roozee, F. M. Bickelhaupt and T. A. Hamlin, *J. Org. Chem.*, 2022, **87**, 1805–1813.
- 26 G. N. Simm, P. L. Türtscher and M. Reiher, *J. Comput. Chem.*, 2020, **41**, 1144–1155.
- 27 T. A. Hamlin, M. Swart and F. M. Bickelhaupt, *ChemPhysChem*, 2018, **19**, 1248.
- 28 R. Wang, X. Shi, K. Li, A. Bunker and C. Li, *Int. J. Biol. Macromol.*, 2023, **242**, 125120.
- 29 D. Bareth, S. Jain, J. Kumawat, D. Kishore, J. Dwivedi and S. Z. Hashmi, *Bioorg. Chem.*, 2024, **143**, 106971.
- 30 G. M. J. Frisch, W. Trucks, H. B. Schlegel, G. E. Scuseria, M. A. Robb, J. R. Cheeseman, G. Scalmani, V. Barone, B. Mennucci, G. A. Petersson, H. Nakatsuji, M. Caricato, X. Li, H. P. Hratchian, A. F. Izmaylov, J. Bloino, G. Zheng, J. L. Sonnenberg, M. J. Frisch, G. W. Trucks, H. B. Schlegel, G. E. Scuseria, M. A. Robb, G. Cheeseman, J. R. Scalmani, V. Barone, B. Mennucci, H. Petersson, G. A. Nakatsuji, M. Caricato, X. Li, H. P. Hratchian, A. F. Izmaylov, J. Bloino, G. Zheng, J. L. Sonnenberg, K. Hada, M. Ehara, M. Toyota, R. Fukuda, J. Hasegawa, M. Ishida, T. Nakajima, Y. Honda, O. Kitao, H. Nakai, T. Vreven, J. E. Montgomery, J. A. Peralta Jr, F. Ogliaro, M. Bearpark, J. J. Heyd, E. Brothers, K. N. Kudin, R. Staroverov, V. N. Kobayashi, K. Normand, J. Raghavachari, A. Rendell, J. C. Burant, S. S. Iyengar, J. Tomasi, M. Cossi, N. Rega, J. M. Millam, M. Klene, J. E. Knox, J. B. Cross, V. Bakken, C. Adamo, J. Jaramillo, R. Gomperts, R. E. Stratmann, O. Yazyev, A. J. Austin, R. Cammi, C. Pomelli, J. W. Ochterski, R. L. Martin, K. Morokuma, V. G. Zakrzewski, G. A. Voth, P. Salvador, S. Dannenberg, J. J. Dapprich, A. D. Daniels, Ö. Farkas, J. B. Foresman, J. V. Ortiz, J. Cioslowski and D. J. Fox, *Gaussian 09, Revision E.01*, Gaussian, 2009.
- 31 Y. Zhao and D. G. Truhlar, *Theor. Chem. Acc.*, 2008, **120**, 215–241.
- 32 T. H. Dunning, K. A. Peterson and A. K. Wilson, *J. Chem. Phys.*, 2001, **114**, 9244–9253.
- 33 R. A. Kendall, T. H. Dunning and R. J. Harrison, *J. Chem. Phys.*, 1992, **96**, 6796–6806.
- 34 G. Koleva, B. Galabov, J. Kong, H. F. Schaefer and P. v. R. Schleyer, *J. Am. Chem. Soc.*, 2011, **133**, 19094–19101.



35 F. C. Hill, L. K. Sviatenko, L. Gorb, S. I. Okovytyy, G. S. Blaustein and J. Leszczynski, *Chemosphere*, 2012, **88**, 635–643.

36 M. M. Lawal, T. Govender, G. E. M. Maguire, H. G. Kruger and B. Honarpourvar, *Int. J. Quantum Chem.*, 2018, **118**, e25497.

37 R. Sure, M. E. Mahdali, A. Plajer and P. Deglmann, *J. Comput.-Aided Mol. Des.*, 2021, **35**, 473–492.

38 A. P. Bento, M. Solà and F. M. Bickelhaupt, *J. Comput. Chem.*, 2005, **26**, 1497–1504.

39 M. W. Li and P. M. Zimmerman, *J. Comput. Chem.*, 2018, **39**, 2153–2162.

40 S. Simon, M. Duran and J. J. Dannenberg, *J. Chem. Phys.*, 1996, **105**, 11024–11031.

41 S. F. Boys and F. Bernardi, *Mol. Phys.*, 1970, **19**, 553–566.

42 J. A. Plumley and J. J. Dannenberg, *J. Comput. Chem.*, 2011, **32**, 1519–1527.

43 C. Bannwarth, S. Ehlert and S. Grimme, *J. Chem. Theory Comput.*, 2019, **15**, 1652–1671.

44 K. Fukui, *Acc. Chem. Res.*, 1981, **14**, 363–368.

45 D. A. McQuarrie and J. Simon, *Physical Chemistry: A Molecular Approach*, University Science Books, 1997.

46 H. M. Cezar, S. Canuto and K. Coutinho, *Int. J. Quantum Chem.*, 2019, **119**, e25688, DOI: [10.1002/qua.25688](https://doi.org/10.1002/qua.25688).

47 H. M. Cezar, S. Canuto and K. Coutinho, *J. Chem. Inf. Model.*, 2020, **60**, 3472–3488.

48 J. Tomasi, B. Mennucci and E. Cancès, *J. Mol. Struct.: THEOCHEM*, 1999, **464**, 211–226.

49 K. B. Wiberg, *J. Am. Chem. Soc.*, 1968, **90**, 59–63.

50 J. P. Foster and F. Weinhold, *J. Am. Chem. Soc.*, 1980, **102**, 7211–7218.

51 F. M. Bickelhaupt and K. N. Houk, *Angew. Chem., Int. Ed.*, 2017, **56**, 10070–10086.

52 P. Vermeeren, S. C. C. van der Lubbe, C. Fonseca Guerra, F. M. Bickelhaupt and T. A. Hamlin, *Nat. Protoc.*, 2020, **15**, 649–667.

53 A. P. Bento and F. M. Bickelhaupt, *Chem.-Asian J.*, 2008, **3**(10), 1783–1792.

54 X. Sun, T. M. Soini, J. Poater, T. A. Hamlin and F. M. Bickelhaupt, *J. Comput. Chem.*, 2019, **40**, 2227–2233.

55 M. H. Abraham and D. J. McLennan, *J. Chem. Soc., Perkin Trans. 2*, 1977, 873, DOI: [10.1039/p29770000873](https://doi.org/10.1039/p29770000873).

56 R. E. Robertson, A. Annesa and J. M. W. Scott, *Can. J. Chem.*, 1975, **53**, 3106–3115.

57 R. L. Heppolette and R. E. Robertson, *Can. J. Chem.*, 1966, **44**, 677–684.

58 E. Perlitz, M. von Domaros, B. Kirchner, R. Ludwig and F. Weinhold, *Sci. Rep.*, 2017, **7**, 10244.

59 W. P. Jencks, *Chem. Rev.*, 1985, **85**, 511–527.

60 R. A. M. O'Ferrall, *J. Chem. Soc. B*, 1970, 274–277, DOI: [10.1039/J29700000274](https://doi.org/10.1039/J29700000274).

61 I. Fernández and F. M. Bickelhaupt, *Chem. Soc. Rev.*, 2014, **43**, 4953–4967.

